



Experimental and finite element analyses of seismic behavior of pile-reinforced soft clayey slope

Lei Zhang¹ · Panpan Zhang¹ · Cheng Chen¹ · Zhen Zhang¹ · Rui Rui¹

Received: 5 December 2023 / Accepted: 31 May 2024 / Published online: 13 June 2024
© The Author(s) 2024

Abstract

In this study, a series of shaking table model tests and three-dimensional (3D) finite element (FE) analyses were performed to mainly investigate the seismic deformations of clayey slopes reinforced by different pile configurations. The influences of ground motion intensity and frequency, and flexural rigidity, length and installation location of pile were systematically investigated. For the different pile configurations considered, the pile-cap system was found to be most effective improving the seismic stability of the clayey slope; the frontal piles tended to experience much larger bending moments than the rear piles, exhibiting a clear shadowing effect of the frontal piles. The acceleration amplification factors and maximum relative displacements of monitoring points along the slope surface were found to generally increase with the elevation, which tended to respectively become smaller and more significant with the increasing ground motion intensity. For pile flexural rigidity larger than $6.03 \times 10^5 \text{ kN} \cdot \text{m}^2$, the reinforcement performance of the pile-cap system on the clayey slope under seismic shakings could not be effectively improved; besides, the viable pile length and installation location were proposed for improving the seismic stability of clayey slope reinforced by the pile-cap system.

Keywords Anti-slide pile · Seismic response · Slope stability · Shaking table model test · Clayey slope

Introduction

Numerous studies have shown that catastrophic landslides triggered by earthquakes account for a significant proportion of earthquake-induced disasters (e.g., Parise and Jibson 2000; Jibson et al. 2007; Hsieh and Lee 2011). Earthquake-induced landslides of soft clayey slopes have also been widely reported, such as the Government Hill and Turnagain Heights landslides triggered by the 1964 Alaska earthquake

(Seed 1968; Updike et al. 1988), the Sainte-Thecle and Saint-Adelphe landslides induced by the 1988 Saguenay earthquake in Canada (Lefebvre et al. 1992). As a preventive measure in stabilizing slopes, anti-slide piles have been used successfully in many slopes consisting of different soil or rock types, which can transfer the sliding thrust induced by landslide to rock or more stable soil layers at greater depths (e.g., Chen and Martin 2002; Zeng and Liang 2002; Won et al. 2005; Stamatopoulos et al. 2009 Zhang et al. 2017a, 2024; Nguyen et al. 2018; Olgun et al. 2019; Mao et al. 2019; Wang et al. 2024; Yenginar and Olgun 2023).

Compared to rock or cohesionless soil slopes (e.g., Lin and Wang 2006; Zhao et al. 2020; Yan et al. 2020; Zhang et al. 2020, 2021a; Su et al. 2021; Xu et al. 2022; Liu et al. 2022; Xie et al. 2022; Zhou et al. 2023; Zheng et al. 2024; Peng et al. 2024), the seismic model tests performed on soft cohesive soil slopes with or without reinforcement are relatively scarce; the relevant experimental studies using centrifuge set-up are briefly introduced herein. The seismic responses of five clayey embankment slopes were experimentally investigated by Kutter et al. (1989), in which the influences of earthquake intensity on the acceleration amplification factor and slope failure pattern were discussed. A

✉ Cheng Chen
chengchen87@whut.edu.cn

Lei Zhang
zhangleigeo@whut.edu.cn

Panpan Zhang
zhangpanpan1005@whut.edu.cn

Zhen Zhang
617983080@qq.com

Rui Rui
r.rui@whut.edu.cn

¹ School of Civil Engineering and Architecture, Wuhan University of Technology, Wuhan, Hubei 430070, China

series of seismic model tests on soil-nailing-reinforced steep cutting slope of unsaturated silty clay were performed by Zhang et al. (2001), observing that the seismic deformation behavior and failure mechanism of the soil-nailed slope were influenced significantly by the nail spacing, nail length and inclination of slope; similar findings were observed by Wang et al. (2010) who also experimentally explored the seismic responses of nail-reinforced and unreinforced cohesive soil slopes. The seismic behavior of cohesive soil slope reinforced by single pile was experimentally examined by Wang and Zhang (2014), in which the displacement and acceleration of the slope, as well as the displacement and bending moment of the stabilizing pile, were analyzed. Park and Kutter (2015) experimentally explore the static and seismic failure mechanisms of moderately to highly sensitive clay slopes, and found that the slip surfaces of the sensitive clay slopes under seismic loading tended to reach deeper depths and yielded a more diffused shear band than that under static load. Tarazona et al. (2020) experimentally explored the seismic behavior of kaolin clay canyons with three different sloping angles (15°, 30° and 45°, respectively), and the influences of terrain condition, input motion frequency and amplitude were examined. Soriano Camelo et al. (2021, 2022) experimentally investigated the seismic response of gently inclined slopes (3° and 6° inclination angles) of soft clay, analyzing the acceleration response and lateral displacement of the slopes subjected to a suite of sinusoidal waves and scaled realistic motions with different amplitudes and intensities. To date, some experiments have been performed to investigate the seismic behavior of clayey slope with and without reinforcement; however, these studies seldom involve the use of piles with different configurations. Hence, to better understand the reinforcement effect of pile on clayey slope subjected to seismic shaking, further experimental studies are still needed.

On the other hand, numerical approaches have been widely employed to investigate the seismic response of clayey slopes. Biscontin and Pestana (2006) performed a series of dynamic finite element analyses to investigate the seismic response of submarine clayey slope, finding that the ground motions with lower frequency content, longer duration tended to cause more significant excess pore pressure and larger permanent deformation of the slope; besides, the earthquake-induced deformations of very gentle clayey slopes (e.g. inclination angle of 2.5°) could be also considerable. Zhou et al. (2017) proposed a disturbance-dependent soil constitutive model for describing nonlinear behavior of sensitive clays subjected to dynamic loads, which was incorporated in the QUIVER code to perform one-dimensional seismic parametric analyses on generic clay slopes with varying sloping angles. Using the two-dimensional finite difference software FLAC, Karray et al. (2018) conducted

both pseudo-static and dynamic analyses on homogeneous clayey slopes under seismic shakings, and safety factors and failure surfaces of the slopes were obtained from these analyses, which were also compared with the relevant 1-g model test results. By employing cyclic elastoplastic constitutive model to depict the dynamic behavior of saturated soft clay and updated Lagrange technology, Mi and Wang (2021) proposed a numerical simulation procedure to analyze the dynamic sliding process of submarine soft clay slope under seismic load using ABAQUS. In addition, some other simplified methods have also been employed to examine the seismic behavior of slope, such as limit equilibrium method (LEM) (e.g., Rodríguez-Ochoa et al. 2015a; Nian et al. 2019) in which the earthquake-induced force was generally accounted for using the pseudo-static method, and Newmark sliding block method to evaluate the accumulated displacement of a slope during an earthquake (Grelle et al. 2011; Yang et al. 2021). As can be seen, although there are some numerical and simplified approaches employed to investigate the seismic stability of clayey slope, the effect of reinforcement measure such as using anti-slide piles is not accounted for.

As can be summarized from the above descriptions, most of the previous experimental and numerical analyses focused on the seismic responses of rock or cohesionless soil slopes; the relevant studies on the response of piled clayey slope, especially considering pile group of varying configurations, are significantly insufficient. Considering that the dynamic behavior of soil and dynamic soil-structure interaction are highly dependent on the soil type, the seismic performance of seldom investigated pile-reinforced clayey slope is largely unknown. Hence, some relevant investigations are needed to well understand the behavior of pile-reinforced clayey slope under seismic shakings. In this study, a series of 1-g shaking table tests were performed to investigate the seismic performance of pile-reinforced clayey slope subjected to far-field ground motions, taking into account the variations in pile configuration and ground motion parameters. Subsequently, the rationality of three-dimensional (3D) dynamic finite element (FE) analyses were validated by the experimental results; moreover, a suite of numerical parametric analyses were conducted to for further extended investigations, from which some viable suggestions on using anti-slide piles to improve the seismic stability of inclined soft clay ground can be drawn.

Table 1 Basic parameters of the soft clay

Parameter	Value
Density (g/cm ³)	1.6
Water content (%)	60.2
Liquid limit (%)	75.6
Plastic limit (%)	42.1
Effective Poisson's ratio	0.3
Initial void ratio	1.64
Compression index	0.546
Coefficient of permeability (m/s)	$2.74 \times 10^{-9} \sim 4.25 \times 10^{-8}$
Effective frictional angle	23°
Recompression index	0.12
Small-strain modulus (kPa)	$2060(p_0')^{0.653}$

Note p_0' is the initial mean effective normal stress, with the unit of kPa; the formula of small-strain modulus is developed by Banerjee et al. (2014)

Table 2 Similarity ratio relationships adopted in present 1-g shaking table test

Physical parameters		Similar conditions	Similarity constant
Geometric parameters	Length (l)	C_l	1/50
	Displacement (s)	$C_s = C_l$	1/50
Material properties	Density (ρ)	C_ρ	1
	Unit weight (γ)	C_γ	1
	Strain (ε)	C_ε	1
Dynamic characteristics	Stress (σ)	$C_\sigma = C_\rho \cdot C_l$	1/50
	Input acceleration (a)	C_a	1
	Time (t)	$C_t = (C_a/C_l)^{-1/2}$	$50^{-1/2}$
	Frequency (f)	$C_f = (C_a/C_l)^{1/2}$	$50^{1/2}$
	Velocity (v)	$C_v = C_l^{1/2}$	$50^{-1/2}$

Test material and methodology

Test model construction

The earthquake model tests were performed using the 1-g shaking table set-up at the Wuhan University of Technology. The clay slurry was mixed in a de-airing chamber containing Malaysia kaolin clay powder and water in a mass ratio of 1:1.2 for around 4 h. To prevent the leakage of clay slurry, a flexible and thin rubber bag was placed inside the shear box with internal dimensions of 900 mm (length) × 600 mm (width) × 400 mm (height). The clay slurry was then placed into the rubber bag, with a lightweight wooden mold to form the shape of the slope. The clay slurry was then subjected to 1-g consolidation process for about 14 days to stabilize the settlement at clay surface and pore water pressures at selected positions. The basic properties of the clay sample are listed in Table 1. In small-scale model tests, to satisfy all the similarity conditions is extremely challenging and often unfeasible. In this study, with reference to previous

1-g shaking table tests (Meymand 1998; Liu et al. 2017; Wu et al. 2022; Haeri et al. 2023; Jia et al. 2023; Pan et al. 2023), the key similarity ratios of geometric parameters, initial stress conditions and dynamic characteristics are designed according to the Buckingham π theorem, as shown in Table 2. Notwithstanding some unavoidable inconsistencies between the prototype and model materials, the present 1-g shaking table tests can provide useful findings revealing the influencing trends of some important factors, which can also be employed to validate a reliable numerical analysis procedure for extended investigations.

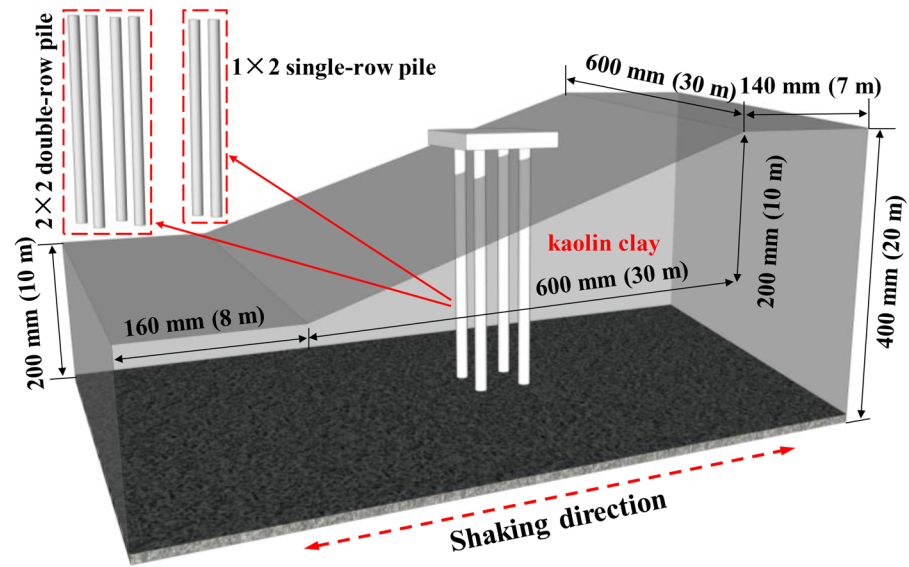
As Fig. 1 shows, three types of pile configuration were employed, namely 1×2 single-row piles, 2×2 double-row piles, and 2×2 pile-cap system, with a pile spacing of 64 mm (4 times the pile diameter). The model piles were gradually inserted into the fully consolidated soft clay bed. The model piles were made of thin-walled aluminum alloy tubes with a length of 320 mm (16 m prototype), a wall thickness of 3 mm (0.15 m prototype), and an outer diameter of 16 mm (0.8 m prototype), the basic properties of pile are shown in Table 3. The pile cap was made of a rectangular aluminum block with dimensions of 128 mm × 128 mm × 20 mm, which was rigidly connected to the model piles by welding, as shown in Fig. 2.

Instrumentation and input ground motions

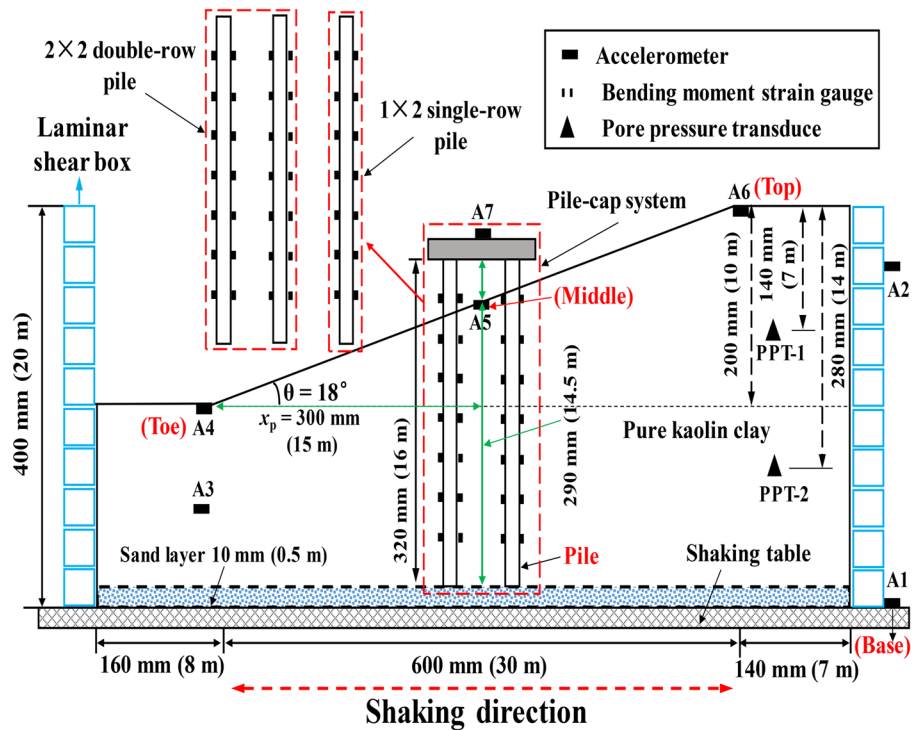
As shown in Fig. 2, several full-bridge strain gauges (strain gauges S1-S7, with sensitivity coefficient of ±1%) were attached to the anti-slide piles to measure the respective bending moment responses during the seismic shakings. A total of 7 horizontal accelerometers, namely A1~A7, were installed at different locations to measure the acceleration response of the test model. Displacements at the locations of accelerometers were obtained by performing the double integration computations of acceleration versus time. Besides, to monitor the pore water pressure changes during the consolidation stage and the seismic shakings, two pore water pressure transducers (PPT) were installed within the clay sample.

In the model tests, a series of sinusoidal waves with frequencies of 1.0 Hz, 3.5 Hz and 7 Hz and peak values of 0.05 g and 0.1 g were employed as the input ground motions, as shown in Fig. 3. It is noted that peak accelerations of 0.05 g and 0.1 g respectively correspond to the seismic intensity levels 6 and 7 specified in the Chinese code for seismic design of buildings (NSPRC 2010); model scale frequencies ranging from 1 to 7 Hz correspond to prototype frequencies ranging approximately from 0.15 to 1 Hz, which fall within the dominant frequency range of typical far-field ground motions. Unless otherwise stated, the test results presented in the next section are in model scale.

Fig. 1 Layout of 1-g shaking table model test (number in bracket denotes prototype size). (a) three-dimensional view of pile reinforcement model; (b) elevational view of the model



(a) three-dimensional view of pile reinforcement model



(b) elevational view of the model

Table 3 Basic properties of pile

Poisson's ratio	Density (g/cm ³)	Length (mm)	Elastic modulus (GPa)	Outer diameter (mm)	Thickness (mm)
0.2	2.7	320	70	16	3

Experimental results

Slope failure phenomenon

For peak base acceleration (PBA) equal to 0.05 g, all the slopes with and without pile reinforcement are generally stable throughout the seismic shakings, regardless of

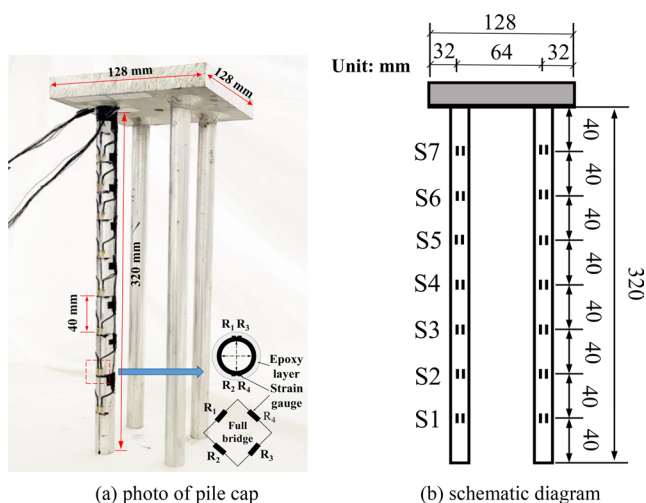


Fig. 2 The model of 2×2 pile-cap system in shaking table test. (a) photo of pile cap; (b) schematic diagram

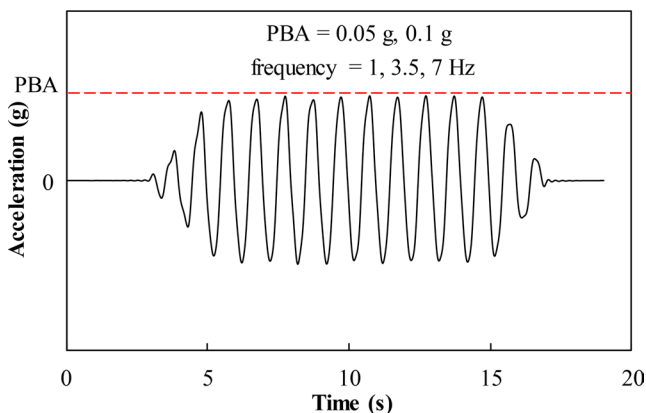


Fig. 3 Input ground motions in shaking table model test (frequencies are 1 Hz, 3.5 Hz and 7 Hz, PBA denotes peak base acceleration)

the shaking frequencies. For PBA equal to 0.1 g, as demonstrated in Fig. 4(a) and 4(b), after the seismic shakings obvious slope slide occurs for the unreinforced and 1×2 single-row-pile reinforced slope models. For the slope models reinforced by 2×2 double-row piles and pile-cap system, such slope slides are not observed, as Fig. 4(c) and 4(d) show; however, the piles generally become tilted due to downslope kinematic force imposed by the clays. Hence, for pile-reinforced clayey slope, the seismic stability of which is highly dependent on the pile reinforcement configuration.

Acceleration response

Typical measured acceleration time histories at different locations of slope are presented in Fig. 5, in which the accelerations of the slope toe, slope middle and slope top are measured by the accelerometers A4, A5 and A6 respectively. As can be seen, for all of the test models, the accelerations experienced at different locations of slope are clearly larger

than that excited at the slope model base, indicating the evident amplification effect of soft clay on seismic ground motions (Tinawi et al. 1993; Mayoral et al. 2009; Banerjee et al. 2014; Garala and Madabhushi 2019; Soriano Camelo et al. 2022). Moreover, the acceleration responses of the unreinforced slope are relatively more significant.

The acceleration amplification factor in this study is defined as the ratio of the peak acceleration experienced at a selected location to that excited at the model base. Figure 6 gives the detailed comparison curves of acceleration amplification factor for slope models without and with different pile reinforcement configurations, in which h/H represents the relative height; it is defined as the ratio of the height of a certain measuring point to the total height of the slope, measured from the slope toe. As can be seen, for all the scenarios considered, the acceleration amplification factor along the slope surface gradually increases with the increasing elevation. In comparison, the amplification effect of slope surface is more significant for shaking frequency equal to 7 Hz than that involving the other two frequencies; the acceleration responses of slopes reinforced by anti-slide piles are suppressed in different degrees compared with the unreinforced slope. For shaking frequency equal to 7 Hz and PBA=0.05 g, the acceleration amplification factor at slope top for the unreinforced slope is 2.83, while that associated with the pile reinforcement configurations of 1×2 single-row piles, 2×2 double-row piles, and 2×2 pile-cap system are respectively 10%, 15% and 20% smaller.

Maximum relative displacement

Figure 7 presents the maximum relative displacements at different locations of the slope surface. The maximum relative displacement is defined as the maximum value of relative displacement between a monitoring point and model base during a specific seismic shaking, along the horizontal shaking direction. As can be seen from Fig. 7, for the same ground motion intensity, the maximum relative displacements of the slopes reinforced by anti-sliding piles are significantly smaller compared to that of unreinforced slope, which tend to be evidently influenced by the shaking frequency and intensity. For PBA equal to 0.1 g and shaking frequency equal to 1 Hz, the maximum relative displacement experienced at the top of unreinforced slope is the about 3 cm, while that associated with 2×2 pile-cap system is 42% smaller.

Typical excess pore water pressure response

Two pore pressure transducers, namely PPT-1 and PPT-2 located respectively at depths of 140 mm (7 m prototype depth) and 280 mm (14 m prototype depth) below the

Fig. 4 Photos of test samples after seismic shaking (PBA=0.1 g, frequency=1 Hz). (a) unreinforced slope; (b) slope reinforced with 1×2 single-row piles; (c) slope reinforced with 2×2 double-row piles; (d) slope reinforced with 2×2 pile-cap system

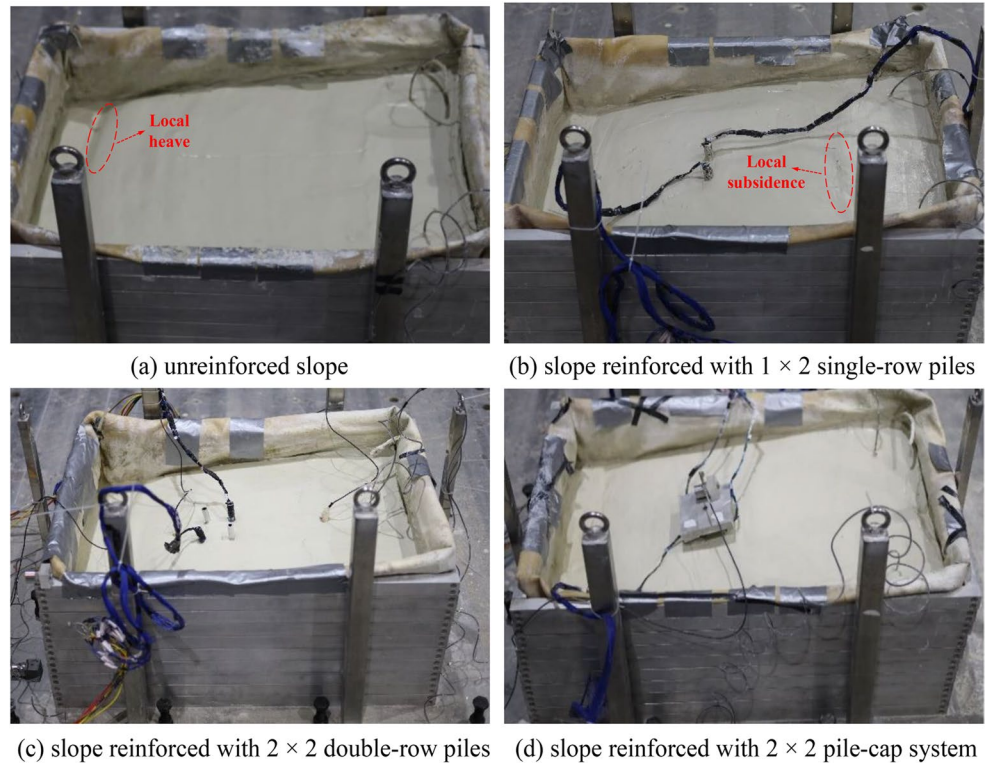
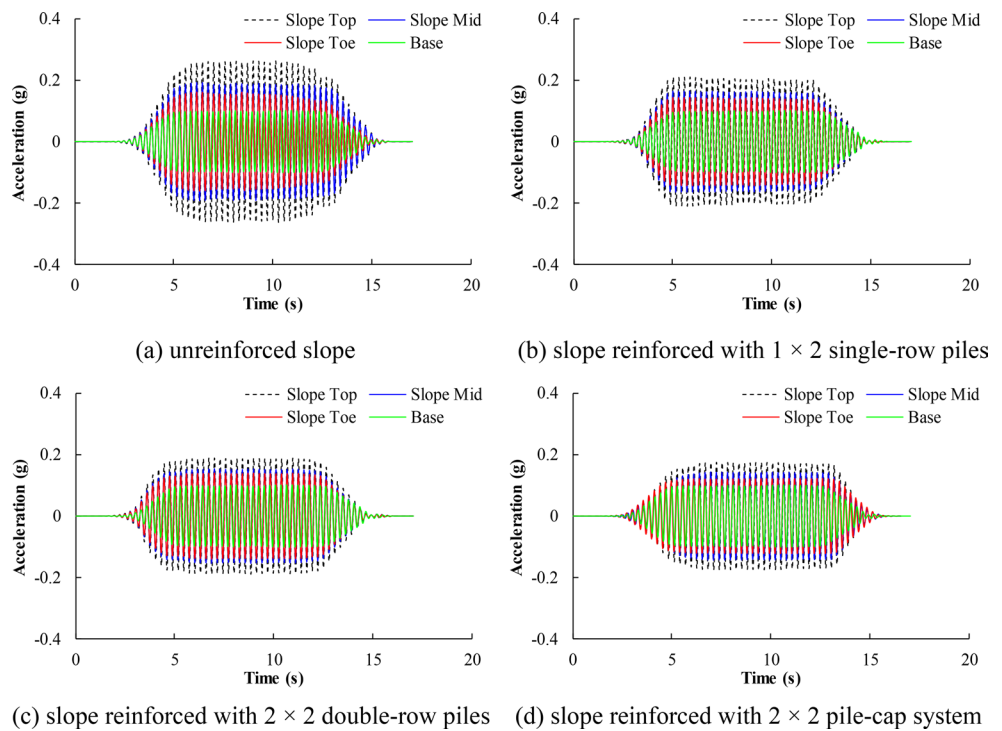


Fig. 5 Acceleration time histories at different positions of slopes reinforced by different anti slide piles (PBA=0.1 g, frequency=3.5 Hz). (a) unreinforced slope; (b) slope reinforced with 1 × 2 single-row piles; (c) slope reinforced with 2 × 2 double-row piles; (d) slope reinforced with 2 × 2 pile-cap system



clay surface in shaking table model tests, respectively, were employed to monitor the excess pore water pressure response in the clay during seismic shakings.

Figures 8 and 9 respectively present the typical time histories of excess pore water pressure for both unreinforced clay slope and clay slope reinforced with pile-cap system

subjected to different seismic shakings. As can be seen, although there are some local discrepancies, the variation trends of excess pore water pressure are generally comparable between unreinforced and reinforced clay slopes; under the same seismic loadings, the excess pore water pressures generated in the reinforced clay slope are slightly smaller,

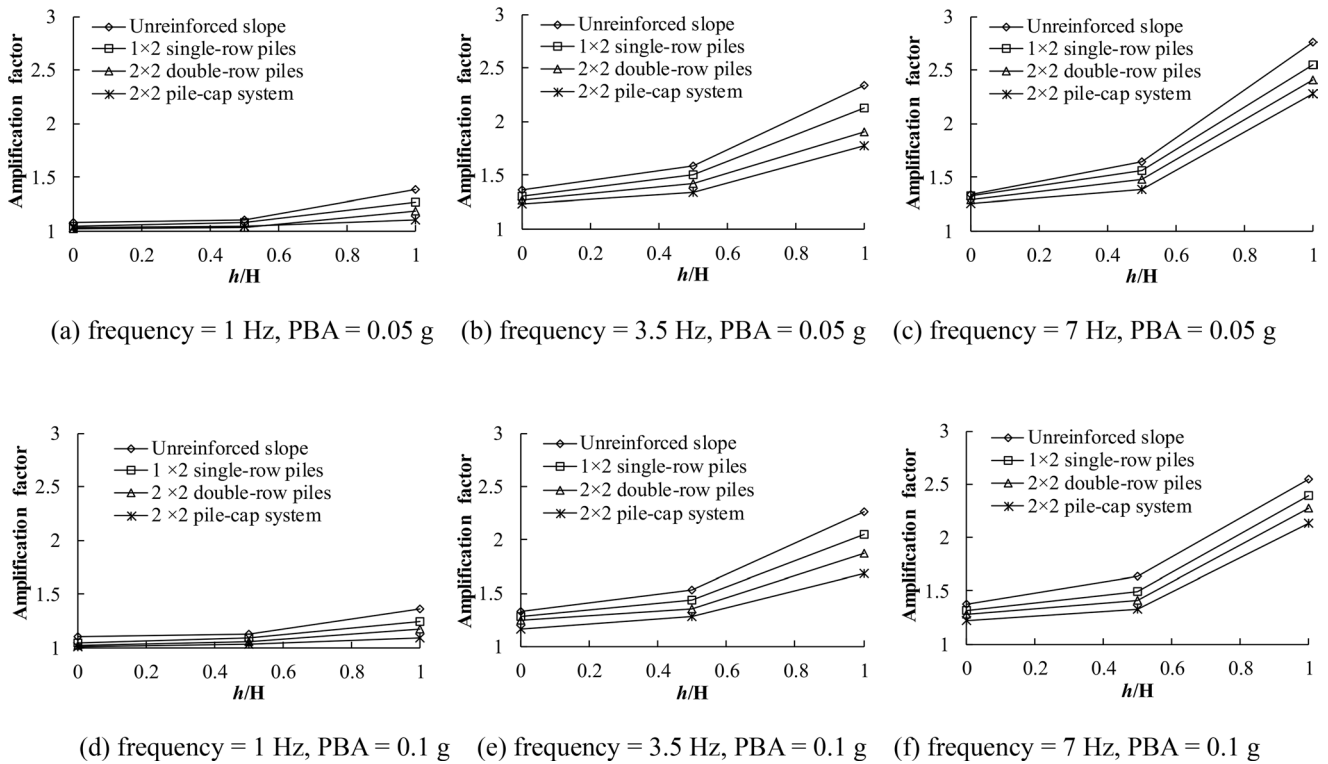


Fig. 6 Plots of acceleration amplification factor for slopes reinforced by different anti slide piles (h/H denotes relative height). (a) frequency=1 Hz, PBA=0.05 g; (b) frequency=3.5 Hz, PBA=0.05 g; (c) frequency=7 Hz, PBA=0.05 g; (d) frequency=1 Hz, PBA=0.1 g; (e) frequency=3.5 Hz, PBA=0.1 g; (f) frequency=7 Hz, PBA=0.1 g

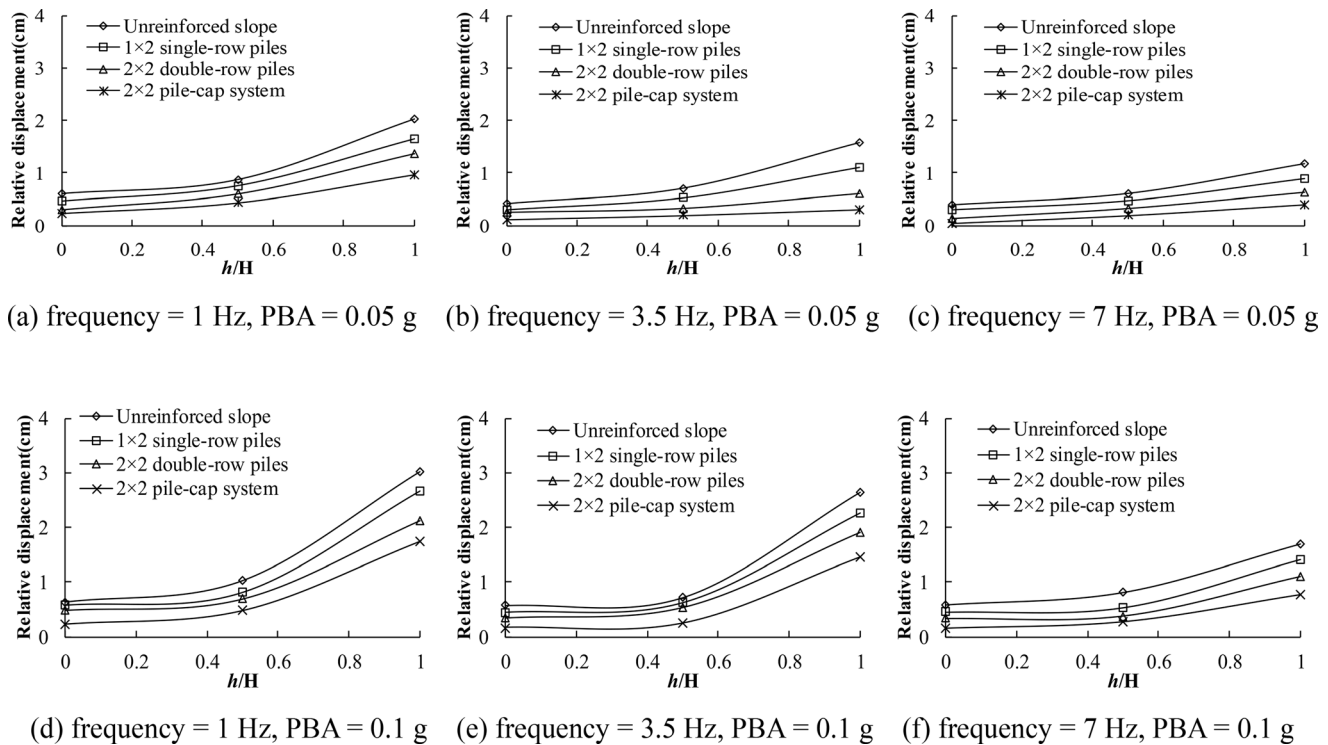


Fig. 7 Maximum relative displacements of slope after seismic shakings. (a) frequency=1 Hz, PBA=0.05 g; (b) frequency=3.5 Hz, PBA=0.05 g; (c) frequency=7 Hz, PBA=0.05 g; (d) frequency=1 Hz, PBA=0.1 g; (e) frequency=3.5 Hz, PBA=0.1 g; (f) frequency=7 Hz, PBA=0.1 g

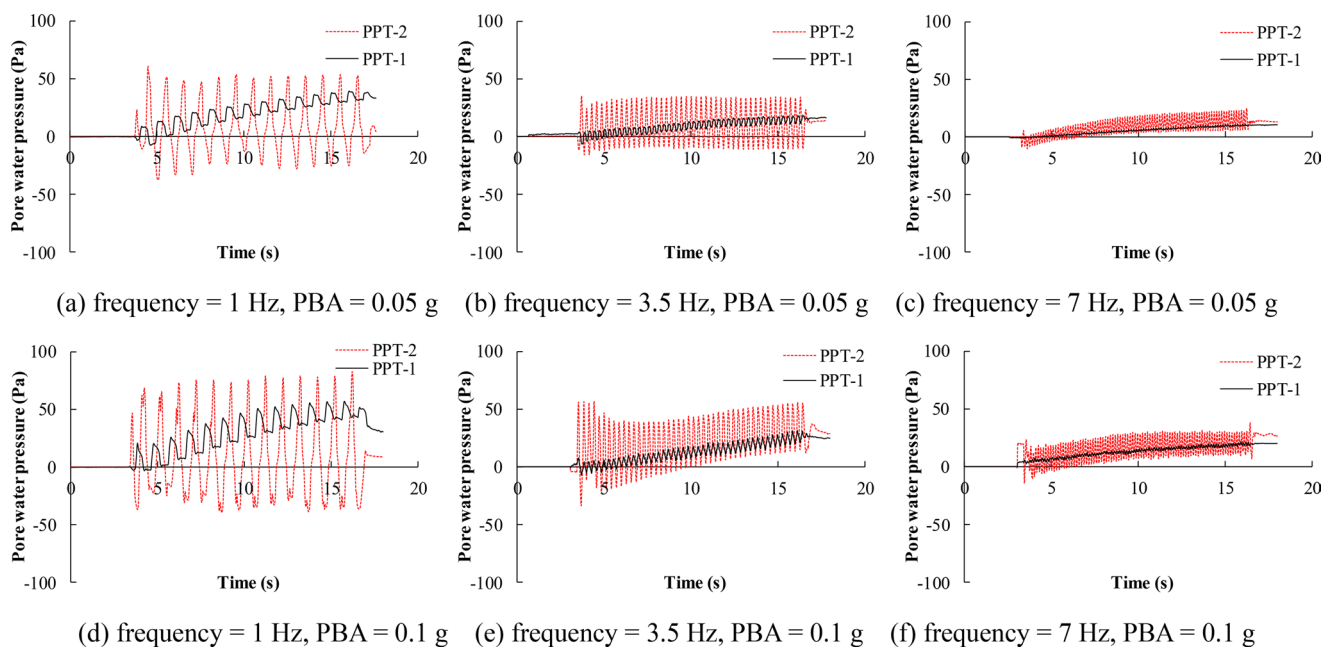


Fig. 8 Typical PPT readings during different ground motions for the unreinforced clay slope. (a) frequency=1 Hz, PBA=0.05 g; (b) frequency=3.5 Hz, PBA=0.05 g; (c) frequency=7 Hz, PBA=0.05 g; (d) frequency=1 Hz, PBA=0.1 g; (e) frequency=3.5 Hz, PBA=0.1 g; (f) frequency=7 Hz, PBA=0.1 g

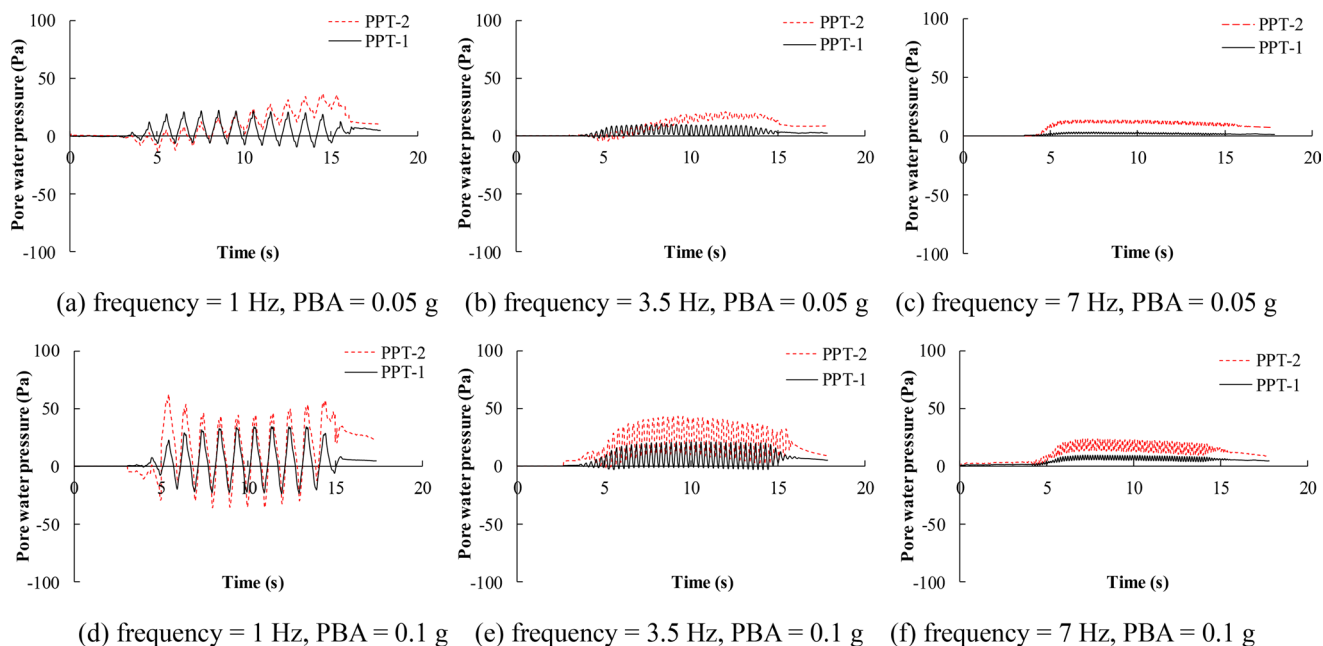


Fig. 9 Typical PPT readings during different ground motions for the clay slope reinforced with 2x2 pile-cap system. (a) frequency=1 Hz, PBA=0.05 g; (b) frequency=3.5 Hz, PBA=0.05 g; (c) frequency=7 Hz, PBA=0.05 g; (d) frequency=1 Hz, PBA=0.1 g; (e) frequency=3.5 Hz, PBA=0.1 g; (f) frequency=7 Hz, PBA=0.1 g

indicating that the excess pore water pressure response in clay slope is not significantly influenced by pile reinforcement. Moreover, the variations in excess pore water pressure tend to be more evident for a deeper depth or a stronger shaking intensity, which become relatively less significant with the shaking frequency changing from 1 Hz to 7 Hz; this

decreasing trend is consistent with that shown in Fig. 7 of maximum relative displacement of slope involving different shaking frequencies. However, in all the test cases, due to the low permeability of saturated kaolin clay and its insensitivity of volumetric change to horizontal seismic shakings, the accumulated excess pore water pressures are rather low

compared to the respective hydrostatic pressures. Hence, the effects of excess pore water pressure accumulation and dissipation are relatively insignificant for the kaolin clay bed subjected to small to medium seismic shakings.

Typical pile bending moment response

The focus of this study is mainly placed on the seismic response of slope. In this section, the seismic bending moment response of the pile-cap system is presented. Figure 10 presents the maximum pile bending moment profiles for both the frontal and rear piles, where the frontal and rear piles are differentiated as nearer to the slope top and toe, respectively. The maximum pile bending moment profile refers to the instantaneous pile bending moment profile

at the instant when the uppermost strain gauge attains its maximum value. As can be seen, the seismic pile bending moment can be considerably influenced by both shaking frequency and intensity. For the shaking frequency equal to 1 Hz and PBA increasing from 0.05 g to 0.1 g, the corresponding maximum bending moments of the frontal pile are approximately 31% and 27% smaller, respectively. Hence, for the clayey slope reinforced by the 2×2 pile-cap system, the frontal piles bear significantly more downward thrust load during the seismic shakings.

In addition, regardless of the frontal or rear piles, the pile bending moments are the largest in the case of 1 Hz compared to other two frequencies. This is consistent with the findings shown in Fig. 7, which demonstrates that the

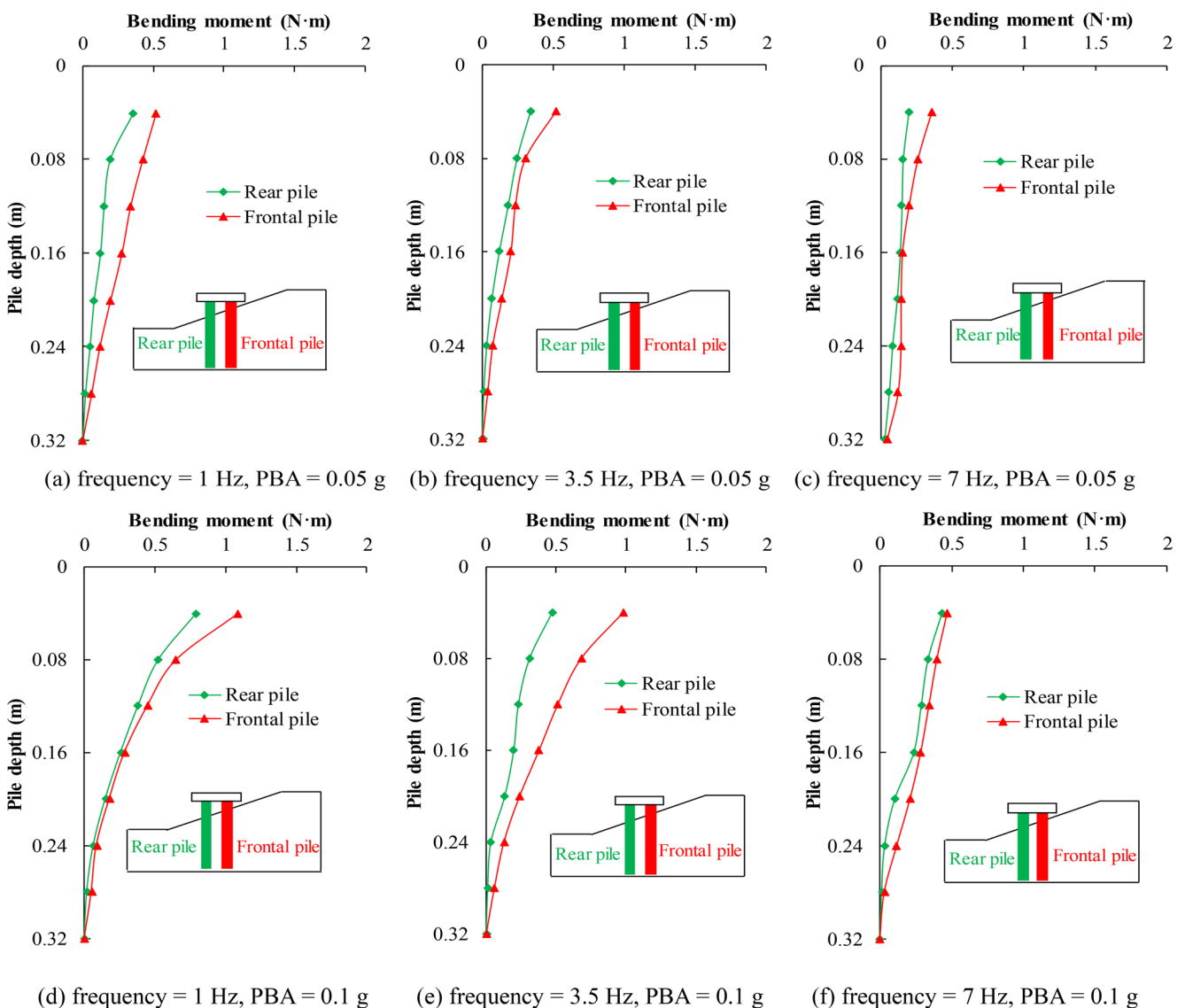
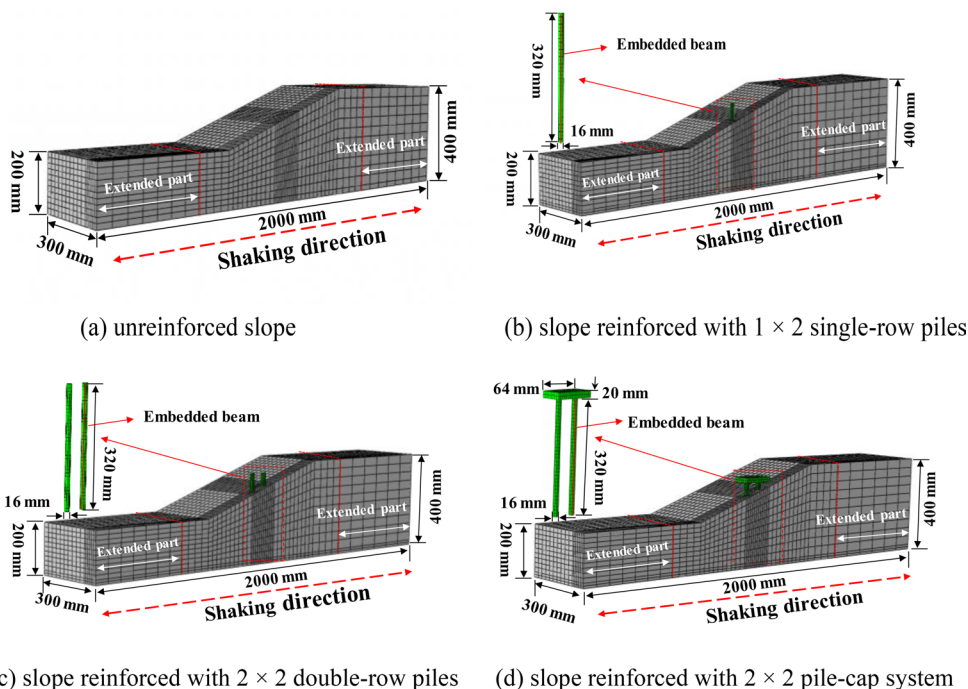


Fig. 10 Maximum pile bending moment profiles for the 2×2 pile-cap system. (a) frequency=1 Hz, PBA=0.05 g; (b) frequency=3.5 Hz, PBA=0.05 g; (c) frequency=7 Hz, PBA=0.05 g; (d) frequency=1 Hz,

PBA=0.1 g; (e) frequency=3.5 Hz, PBA=0.1 g; (f) frequency=7 Hz, PBA=0.1 g

Fig. 11 Semi-symmetrical finite element models of the slopes. (a) unreinforced slope; (b) slope reinforced with 1×2 single-row piles; (c) slope reinforced with 2×2 double-row piles; (d) slope reinforced with 2×2 pile-cap system



relative displacements between the slope surface and model base are also the largest for the shaking frequency of 1 Hz. Hence, the seismic bending moment response of pile is more dependent on the downward thrust of the clayey slope rather than the motion intensity experienced at the slope surface.

Finite element modelling procedure and validation

Geometric modelling information

To further understand the seismic response of pile-reinforced clayey slope, it is necessary to extend the work via reliable numerical simulations. Three-dimensional (3D) simulations are performed using the finite element (FE) software ABAQUS. Considering the geometric symmetry of the test models along the shaking direction, haft 3D FE models can be established for improving computational efficiency, as illustrated in Fig. 11. The soil finite element model adopts solid elements with a mesh type of C3D8R (8-node linear brick element with reduced integration); the pile foundation adopts a hybrid modeling method, using which the pile bending moments can be conveniently extracted from the embedded beam elements of element type B31 (three-dimensional linear beam element) (Banerjee et al. 2014; Zhang et al. 2017b, c).

The seismic waves are applied at the bottom of the model, and the normal directions of two vertical boundaries parallel to the shaking direction are fixed. To minimize the boundary reflection effect, the distance between the lateral boundaries (left and right sides) of the slope models are appropriately extended. Besides, as also adopted in many previous studies

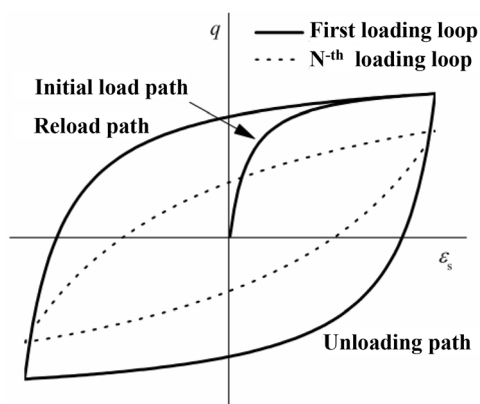


Fig. 12 Schematic diagram of the hyperbolic-hysteretic constitutive soil model

(Banerjee et al. 2014; Tsinidis et al. 2016) to replicate a free-field ground motion condition, the two lateral boundaries of each extended part, which are perpendicular to the shaking direction, are constrained to ensure that nodes at the same elevations have the consistent motions.

Constitutive modelling of soft clay and pile

As demonstrated in Fig. 12, the dynamic behavior of the soft clay is depicted using a hyperbolic-hysteretic constitutive model that is initially proposed by Banerjee et al. (2014), which has been successfully employed to numerically analyze the seismic interaction between clay and various structures (Zhang et al. 2021b; Liu and Zhang 2019); the basic parameters used in this model are listed in Table 1.

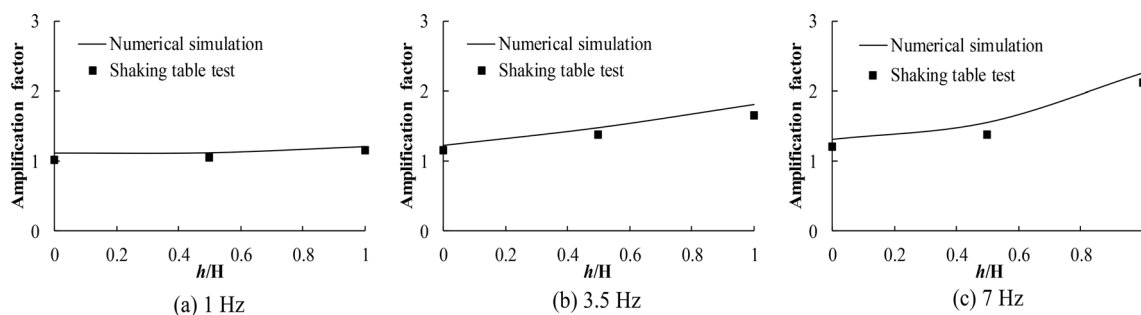


Fig. 13 Comparison of the measured and computed acceleration amplification factors (PBA=0.1 g). (a) 1 Hz; (b) 3.5 Hz; (c) 7 Hz

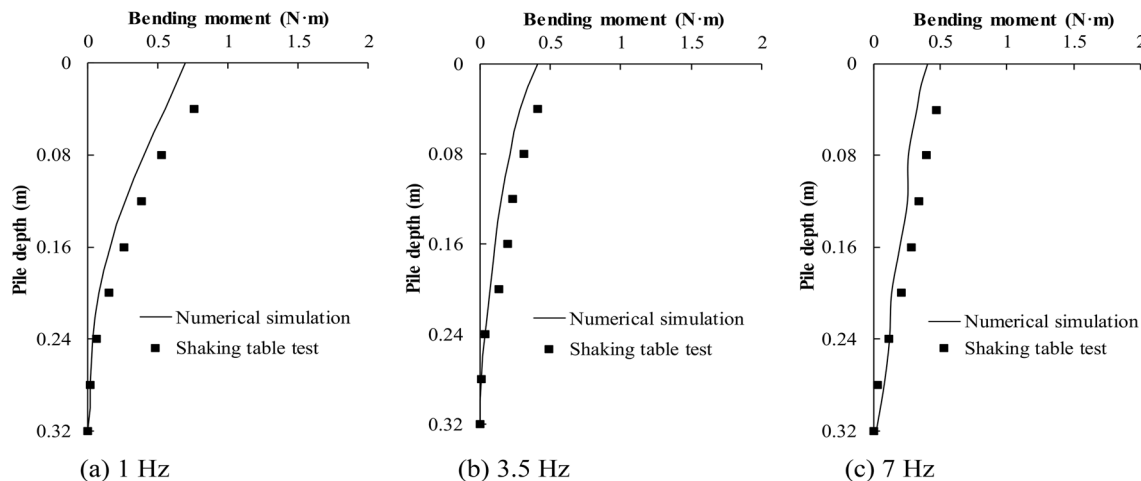


Fig. 14 Comparison of the measured and computed maximum bending moment profiles of rear pile for different shaking frequencies (PBA=0.1 g). (a) 1 Hz; (b) 3.5 Hz; (c) 7 Hz

More detailed information on this model can be found in the study of Banerjee et al. (2014). The ideal linear elastic model is selected for pile and cap involved in this section. In addition, hard-contact and penalty friction algorithms are used to model the behavior of the soil-pile interface, and frictional angle along the interface is taken as 0.8 times that of the clay (e.g., Lin et al. 2023). Rayleigh damping coefficients are applied to the individual piles and pile-cap system, corresponding to a damping ratio of 5% with respect to the first two fundamental frequencies of them.

Validation analysis

Figure 13 exemplifies the comparison between the computed and measured acceleration amplification factors of slope reinforced by the pile-cap-system. As can be seen, the computed and measured acceleration amplification factors at different elevations are generally comparable, and the overall trends of them are quite similar, with the averaged difference generally less than 10%.

Figure 14 plots the corresponding computed and measured maximum pile bending moment profiles involving different shaking frequencies. As can be seen, although

there are some discrepancies between each other, the overall distribution trends of computed and measured bending moments are favorably consistent, with the averaged differences of about 4%, 5% and 8% for shaking frequencies of 1 Hz, 3.5 Hz and 7 Hz, respectively.

The above favorable comparisons between numerical simulation and 1-g shaking table test results confirm that the present 3D FE method can be reliably employed to analyze the pile-reinforced soft clayey slope subjected to ground motions. In the subsequent section, this numerical simulation procedure will be adopted for a suite of numerical parametric analyses for extended investigations.

Numerical parametric analysis

From the model test results, the reinforcement effect of pile-cap system on the clay slope is more significant, and this type of pile configuration is employed in the present parametric analysis. As Fig. 15 shows, using the experimental model of 2×2 pile-cap system as a basis, a series of 3D FE models are established according to the prototype dimensions. The piles in the 2×2 pile-cap system are modelled by an equivalent elastic-plastic model (Zhang et al. 2021b),

Fig. 15 Schematic layout of anti-slide pile reinforced slope model with varying length and installation location of pile

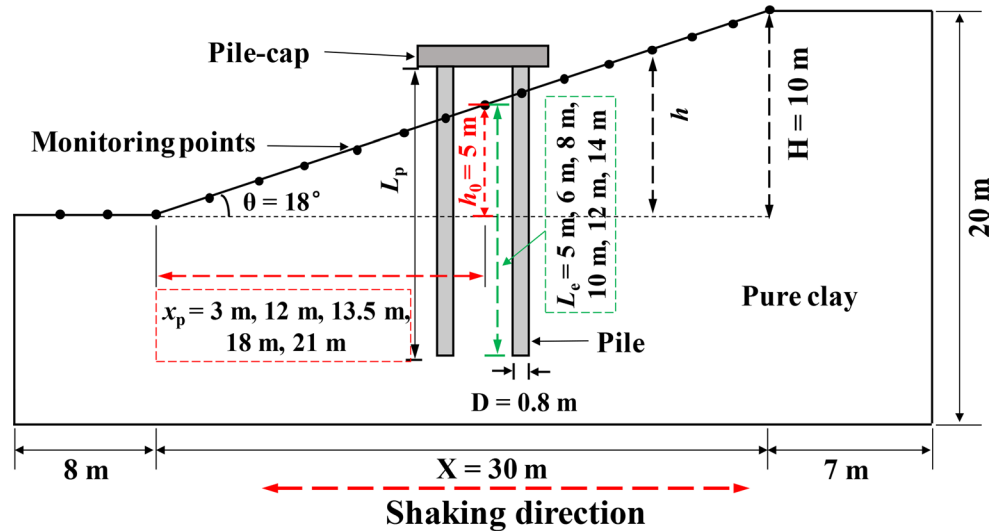


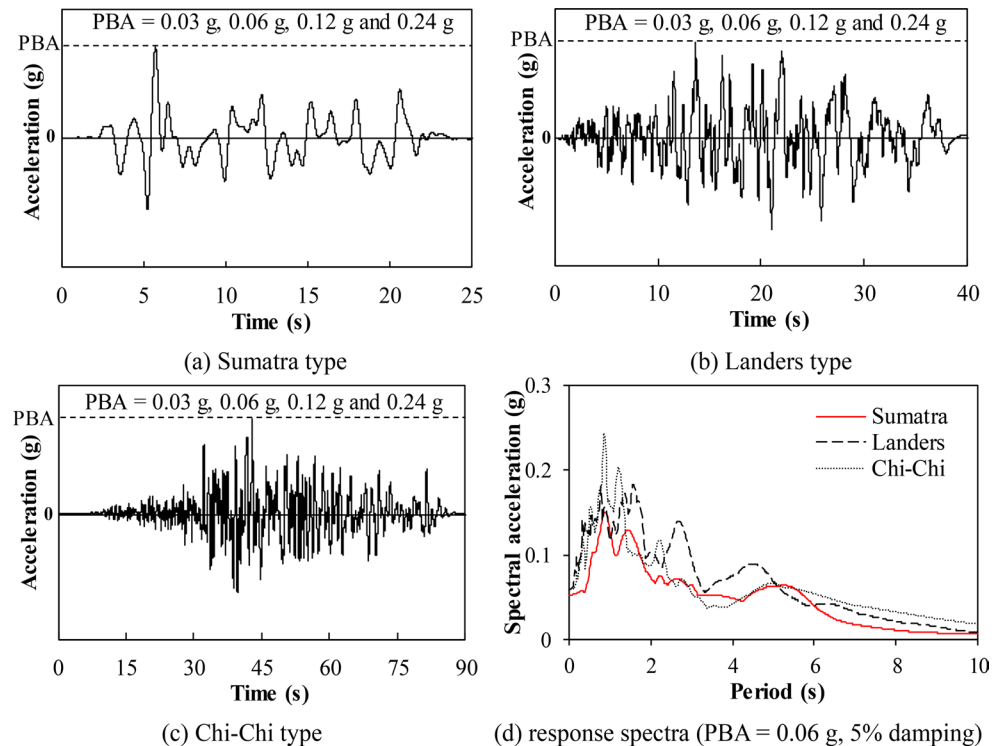
Table 4 Basic properties of pile used in parametric analysis

Density (kg/m ³)	Flexural rigidity(kN·m ²)	Young's modulus (GPa)	Poisson's ratio	Length (m)	Equivalent yield stress (MPa)
2500	1.01 × 10 ⁵ ~1.41 × 10 ⁶	30	0.2	5, 6, 8, 10, 12, 14	15.3

while the rest of the modelling details is the same as that introduced in the preceding section. The basic properties of pile used in parametric analysis are shown in Table 4, and the pile cap share the same elastic properties of pile.

Figure 16 (a)-(c) show the three types of ground motions employed in this section, and the response spectra corresponding to a peak acceleration of 0.06 g are plotted in Fig. 16 (d). The dominant frequencies of these three types of ground motions are all about 1 Hz, representing the typical ground motions that can be experienced at a far field. Detailed information on these ground motions can be found in the study of Zhang and Liu (2018). Furthermore, to investigate the influence of ground motion intensity, each of these base motions was scaled into four ground motions with peak values of 0.03 g, 0.06 g, 0.12 g and 0.24 g.

Fig. 16 Input ground motions adopted in the parametric analysis. (a) Sumatra type; (b) Landers type; (c) Chi-Chi type; (d) response spectra (PBA=0.06 g, 5% damping)



Influence of ground motion intensity

Figure 17 demonstrates the yield zone contours of both unreinforced slope and reinforced slope with 2×2 pile-cap system at the instant when the pile attains its maximum bending moment, where a shear strain of 0.137% is adopted as the threshold value above which evident plastic deformation of clay is initiated (Banerjee 2010; Banerjee et al. 2014). It should be noted that, for shear strains larger than 0.137%, the shear stress of clay can continually increase against the shear strain; the failure state of clay is reached until the clay experiences its peak shear stress (i.e. shear strength), which normally corresponds to a shear strain larger than 2% for Malaysian kaolin clay. As can be seen, with the increasing ground motion intensity, the yield zone of slope tends to gradually expand for both the unreinforced and reinforced slopes, while the yield zone of slope reinforced by the 2×2 pile-cap system is significantly alleviated. For example, for PBA equal to 0.06 g, evident slope failure can be observed from Fig. 17(b) for the unreinforced slope with a maximum shear strain of about 2.36%, while the yield zone is mainly localized around the slope top for the reinforced slope with a maximum shear strain of about 0.45%, indicating that the 2×2 pile-cap system has a satisfactory performance in stabilizing the clayey slope subjected to seismic shakings. Figure 18 also presents the typical plastic strain contours of pile-cap system subjected to different-intensity ground motions. As can be seen, for PBA equal to 0.03–0.06 g,

plastic deformation of pile is negligible; for PBA equal to 0.12 g, evident plastic deformations can be observed at both the top and lower part of the pile. This suggests that pile-cap system installed in clay slope can be damaged under strong ground motions, and the vulnerable locations appear to be the pile top and lower part of pile.

In the subsequent parts of this study, the influences of several important factors on the acceleration amplification factor and maximum relative displacement of slope are discussed.

Figure 19 plots the acceleration amplification factors and maximum relative displacement distributions of the slope surface (denoted as a_g and S_d in this study, respectively), subjected to Sumatra type ground motions with different PBAs. As consistent with the model test results, both the acceleration amplification factor and maximum relative displacement generally tend to increase nonlinearly with the increasing elevation of the monitoring point. Acceleration amplification factors tend to have decreasing trends with the increasing PBA, regardless of the location of monitoring point, indicating that clay damping ratio gradually becomes more significant with the increasing ground motion intensity.

As Fig. 20 shows, for the three types of ground motions, the amplification factor and maximum relative displacement at slope top tend to gradually decrease and increase with the increasing ground motion intensity, respectively, which can be well represented by best-fit lines with maximum prediction errors less than 20%.

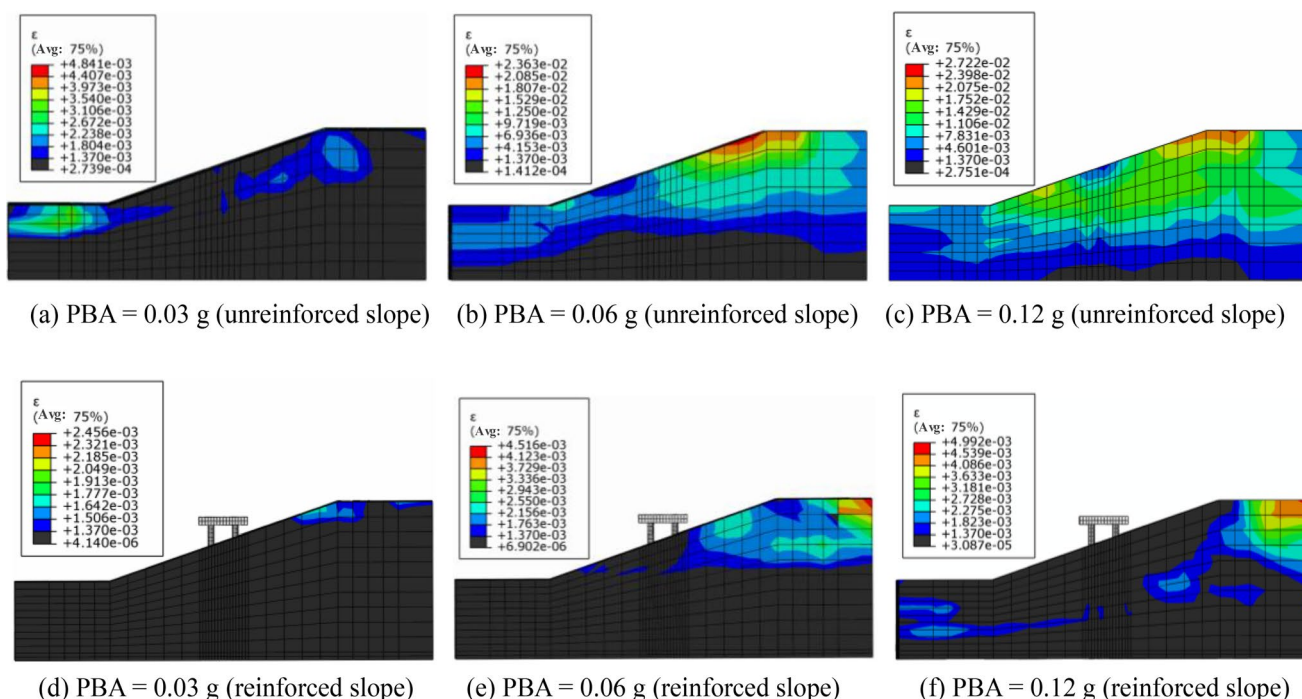


Fig. 17 Yield zone contours of clayey slope at the instant when the frontal pile attains its maximum bending moment, under different-PBA Sumatra-type ground motions (ϵ denotes shear strain). (a) PBA=0.03 g

(unreinforced slope); (b) PBA=0.06 g (unreinforced slope); (c) PBA=0.12 g (unreinforced slope); (d) PBA=0.03 g (reinforced slope); (e) PBA=0.06 g (reinforced slope); (f) PBA=0.12 g (reinforced slope)

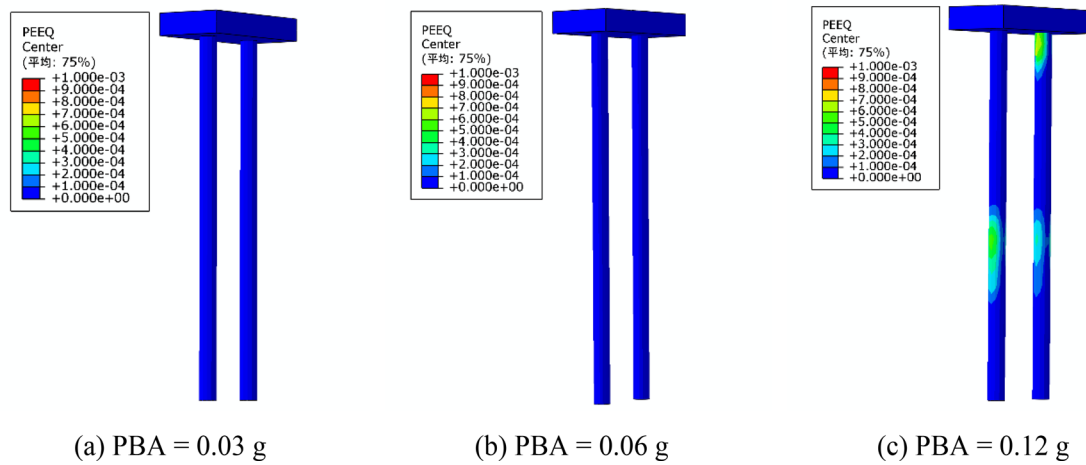


Fig. 18 Equivalent plastic strain (PEEQ) contours of pile-cap system after seismic shakings ($E_p I_p = 6.03 \times 10^5 \text{ kNm}^2$, Sumatra waves). (a) PBA=0.03 g; (b) PBA=0.06 g; (c) PBA=0.12 g

Fig. 19 Plots of acceleration amplification factor and maximum relative displacement of slope surface (Sumatra-type ground motions). (a) acceleration amplification factor; (b) maximum relative displacement

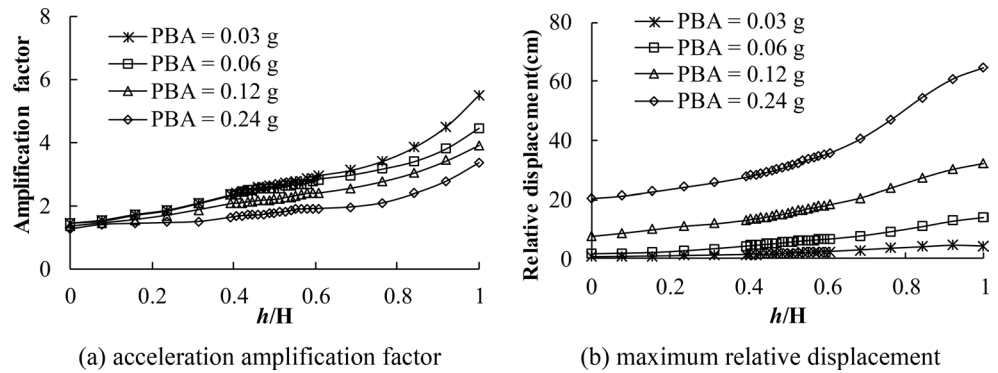
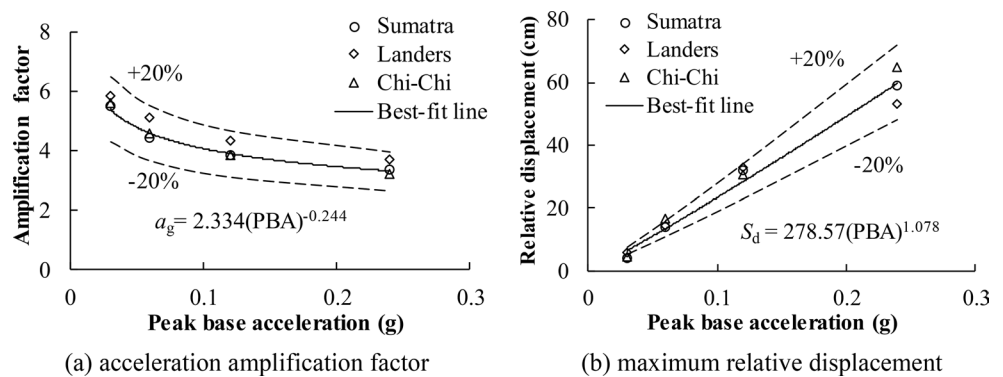


Fig. 20 Influence of PBA on the acceleration amplification factor and maximum relative displacement experienced at slope top. (a) acceleration amplification factor; (b) maximum relative displacement



Influence of pile flexural rigidity

Five different pile flexural rigidities ranging from 1.01×10^5 to $1.41 \times 10^6 \text{ kN}\cdot\text{m}^2$ are considered in this study to explore the influence of pile flexural rigidity (denoted as $E_p I_p$ in this study) on the seismic response of the pile-reinforced clayey slope. As Fig. 21 shows, the larger is the pile flexural rigidity, the smaller are both the acceleration amplification factor and maximum relative displacement of the slope; however, the variation in pile flexural rigidity has no influence on the

increasing trends of both amplification factor and maximum relative displacement against the relative height.

Figure 22 illustrates that both the acceleration amplification factor and maximum relative displacement of the slope top against pile flexural rigidity exhibit a slightly decreasing trend. This is reasonable because the pile with a larger flexural rigidity generally has a better performance in resisting the lateral deformation of slope. Besides, for the three types of ground motions, the acceleration amplification factors and maximum relative displacement at the slope top against pile flexural rigidity can be well represented by respective

Fig. 21 Plots of acceleration amplification factor and maximum relative displacement of slope surface for different pile flexural rigidities (Sumatra-type ground motion, PBA=0.12 g). (a) acceleration amplification factor; (b) maximum relative displacement

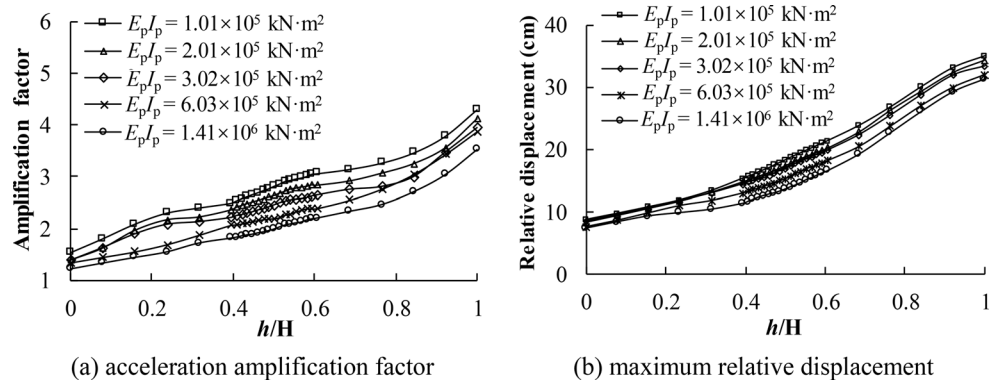


Fig. 22 Influence of pile flexural rigidity on the acceleration amplification factor and maximum relative displacement experienced at slope top (PBA=0.12 g). (a) acceleration amplification factor; (b) maximum relative displacement

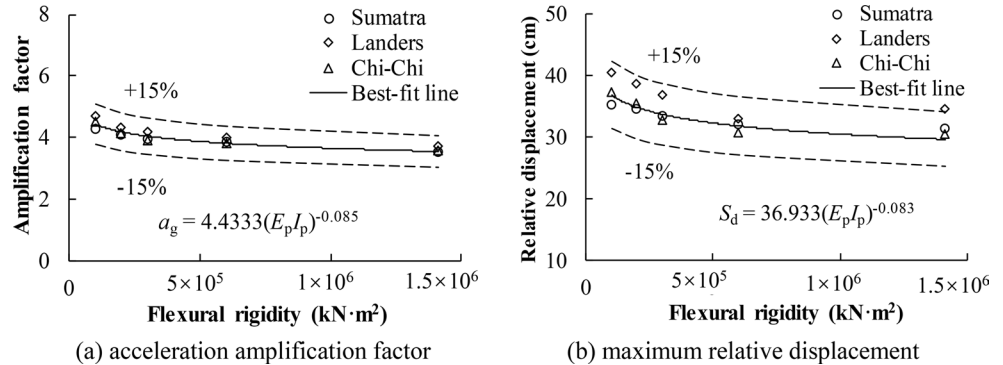
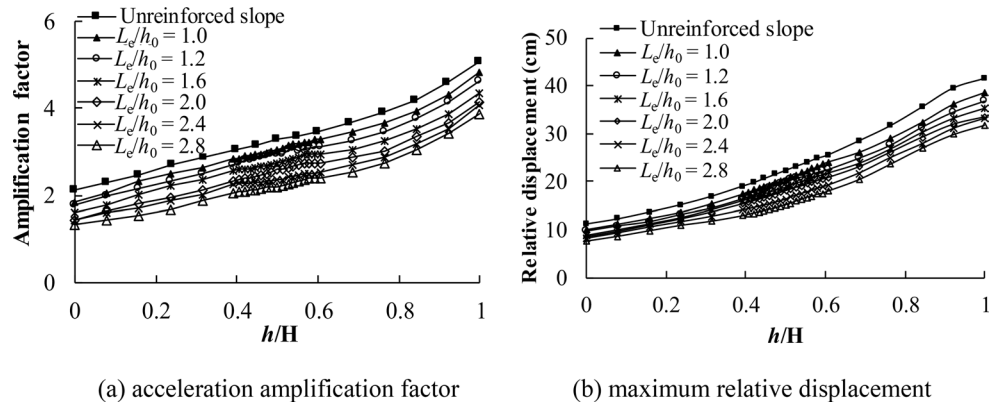


Fig. 23 Plots of acceleration amplification factor and maximum relative displacement of slope surface for different pile lengths (Sumatra-type ground motion, PBA=0.12 g). (a) acceleration amplification factor; (b) maximum relative displacement



best-fit lines with the maximum prediction errors less than 15%.

Influence of pile length

The influence of pile length is considered by varying the embedment depth of pile while the average vertical distance between pile top and slope surface is kept as 2 m. Six different pile embedment depths, viz. $L_e/h_0=1, 1.2, 1.6, 2, 2.4$ and 2.8 , are considered in this subsection, in which L_e and h_0 denote average embedment depth of pile and vertical distance between the pile-surrounded slope surface and slope toe, respectively. As Fig. 23 shows, compared with the unreinforced slope, the acceleration amplification factor and maximum relative displacement of slope surface

with the 2×2 pile-cap system are evidently smaller, which tend to gradually decrease with the increasing pile length. In comparison with the unreinforced slope, for $L_e/h_0=1, 1.2, 1.6, 2, 2.4$ and 2.8 , the averaged acceleration amplification factors of slope surface are respectively 8%, 11%, 17%, 23%, 28% and 32% smaller, and the averaged maximum relative displacements of slope surface are respectively 9%, 13%, 17%, 22%, 26% and 30% smaller. In addition, as Fig. 24 shows, with the increasing pile length, the successive differences in reductions of both acceleration amplification factor and maximum relative displacement of slope appear to be initially increasing and then decreasing. As indicated in Fig. 24, a selection of pile length with average embedment depth of $2 h_0$ is more suitable, which can well

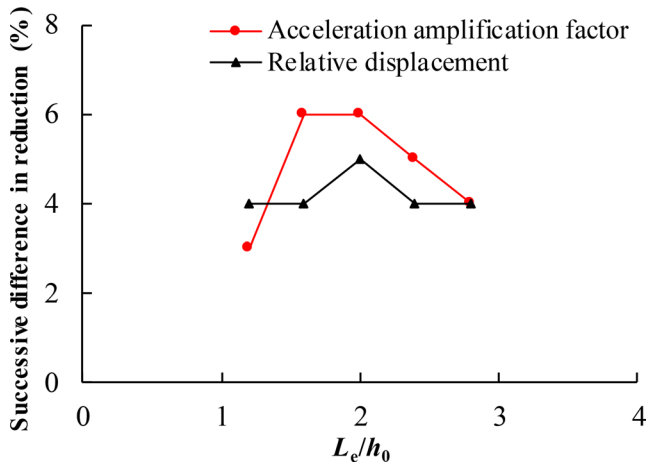


Fig. 24 Successive differences in reductions of acceleration amplification factor and maximum relative displacement of slope surface for different pile lengths (Sumatra-type ground motion, PBA=0.12 g)

balance the reinforcement effect on slope and consumption of pile material.

As Fig. 25 shows, for the three types of ground motions, the amplification factor and maximum relative displacement at slope top tend to gradually decrease with the increasing pile length, and their decreasing trends can be well represented by the respective best-fit lines with the maximum prediction errors less than 15%.

Fig. 25 Influence of pile length on the acceleration amplification factor and maximum relative displacement experienced at slope top (PBA=0.12 g). (a) acceleration amplification factor; (b) maximum relative displacement

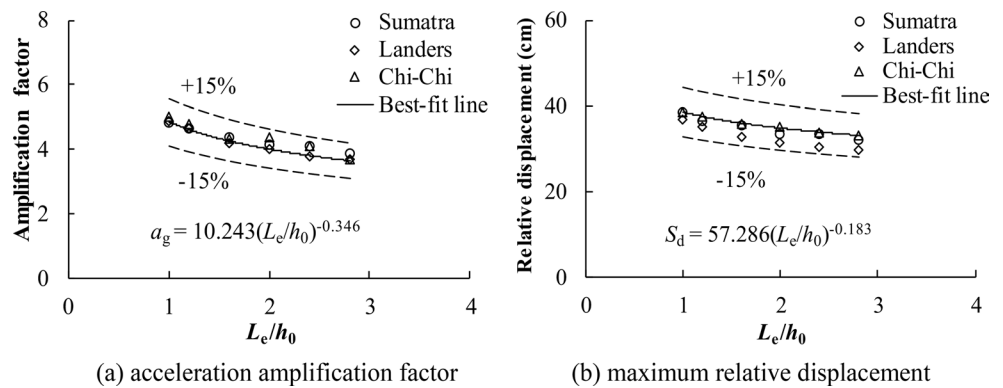
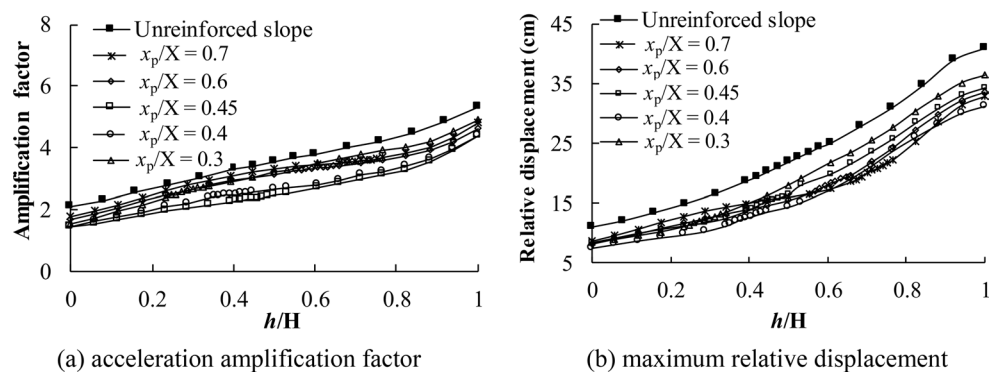


Fig. 26 Plots of acceleration amplification factor and maximum relative displacement of slope surface for different pile locations (Sumatra-type ground motions, PBA=0.12 g, x_p/X represents the pile installation location). (a) acceleration amplification factor; (b) maximum relative displacement



Influence of pile installation location

To explore the influence of pile installation location, denoted as x_p/X in this study, on the seismic response of the pile-reinforced clay slope, five different x_p/X values ranging from 0.3 to 0.7 are considered. As demonstrated in Fig. 15, x_p represents the horizontal distance between the center of pile cap and slope toe, and X represents the horizontal distance between slope toe and top.

The plots of acceleration amplification factor and maximum relative displacement of slope surface are exemplified in Fig. 26. As can be seen, compared with the unreinforced slope, the acceleration amplification factors and maximum relative displacements at different monitoring points can be influenced by the pile installation location to varying degrees. Compared to the acceleration amplification factor, the distribution of maximum relative displacement along the slope surface is more sensitive to the variation of pile installation location. In comparison with the unreinforced slope, for $x_p/X=0.3, 0.4, 0.45, 0.6$ and 0.7 , the averaged acceleration amplification factors of slope surface are respectively 19%, 30%, 32%, 16% and 12% smaller, and the averaged maximum relative displacements of slope surface are respectively 22%, 32%, 23%, 21% and 19% smaller, indicating that the installation location corresponding to $x_p/X=0.4$ is the most efficient for improving the seismic stability of clayey slope.

Conclusions

A series of shaking table model tests were carried out to investigate the seismic responses of clayey slopes reinforced by anti-sliding piles with different configurations. Moreover, a suite of extended 3D FE analyses were performed to further investigate the effects of some important factors on the seismic performance of clayey slope reinforced by pile-cap system, these factors mainly being ground motion intensity, pile flexural rigidity, pile length and pile installation location. The following main conclusions can be drawn:

(1) The 1-g shaking table tests suggest that the soft clay tends to significantly amplify the seismic motions, especially at the location of slope top. Compared with the unreinforced slope, the use of anti-slide piles can evidently reduce the acceleration amplification factor and maximum relative displacement responses of the slope surface due to seismic shakings. Among the different pile configurations considered, the reinforcement effect of the pile-cap system is the most significant, which can substantially reduce the seismic response of the slope and hence improve its seismic stability. For PBA not exceeding 0.1 g, the excess pore water pressure of clay during seismic shakings increases with the increasing seismic intensity or clay depth, but tends to decrease with the increasing shaking frequency; nevertheless, the accumulation or dissipation of excess pore water pressure is quite insignificant compared to the respective hydrostatic pressures.

(2) The acceleration amplification factors and maximum relative displacements for all monitoring points at the slope surface generally increase nonlinearly with the increasing elevation, regardless of the configurations of anti-slide piles. The maximum relative displacements of monitoring points increase significantly with the increasing ground motion intensity while the corresponding acceleration amplification factors tend to have the decreasing trends. For the slope reinforced by the 2×2 pile-cap system, the frontal piles (nearer to the slope top) tend to experience considerably larger downward thrust force than the rear piles, suggesting a shadowing effect existing within the pile group.

(3) The extended numerical parametric studies suggest that, in addition to the pile group configuration, the flexural rigidity, length and installation location of pile also have substantial effects on the seismic response of clayey slope reinforced by pile-cap system. With the increasing pile flexural rigidity, both the acceleration amplification factor and maximum relative displacement of slope surface tend to have decreasing trends; for pile flexural rigidity larger than around $6.03 \times 10^5 \text{ kN} \cdot \text{m}^2$, the decreasing trends become negligible. Moreover, a pile length with an average embedment depth of $2 h_0$ and installation location corresponding to $x_p/X = 0.4$ are found to be favorably efficient for improving

the seismic performance of clayey slope reinforced by the pile-cap system.

Nevertheless, only relatively stiff piles and moderate far-field ground motions are considered in the present 1-g shaking table tests, and the variations in geometric configuration of clayey slope are not accounted for in both the experimental and numerical investigations. Some more factors can be considered in a future study to systematically investigate the elastic-plastic behavior, stability and failure evolution pattern of the piled clayey slope subjected to strong ground motions.

Acknowledgements The authors greatly acknowledge the financial support provided by the National Natural Science Foundation of China (Grant No. 52178353, 51808421).

Funding The presented study is funded by the National Natural Science Foundation of China (Grant No. 52178353, 51808421).

Data availability The data that supports the findings of this research are available from the corresponding author, Cheng Chen, upon a reasonable request.

Declarations

Ethical approval We declare that this manuscript is an original manuscript, which has not been published previously, and not under consideration for publication elsewhere, in whole or in part.

Conflict of interest The authors declare that they have no known competing financial interests or personal relationships that could have appeared to influence the work reported in this paper.

Open Access This article is licensed under a Creative Commons Attribution 4.0 International License, which permits use, sharing, adaptation, distribution and reproduction in any medium or format, as long as you give appropriate credit to the original author(s) and the source, provide a link to the Creative Commons licence, and indicate if changes were made. The images or other third party material in this article are included in the article's Creative Commons licence, unless indicated otherwise in a credit line to the material. If material is not included in the article's Creative Commons licence and your intended use is not permitted by statutory regulation or exceeds the permitted use, you will need to obtain permission directly from the copyright holder. To view a copy of this licence, visit <http://creativecommons.org/licenses/by/4.0/>.

References

- Banerjee S (2010) Centrifuge and numerical modelling of soft clay-pile-raft foundations subjected to seismic shaking. PhD thesis, National University of Singapore, Singapore
- Banerjee S, Goh SH, Lee FH (2014) Earthquake-induced bending moment in fixed-head piles in soft clay. *Geotechnique* 64(6):431–446
- Biscontin G, Pestana JM (2006) Factors affecting seismic response of submarine slopes. *Nat Hazards Earth Syst Sci* 6(1):97–107
- Chen CY, Martin GR (2002) Soil-structure interaction for landslide stabilizing piles. *Comput Geotech* 29(10):363–386

- Garala TK, Madabhushi GSP (2019) Seismic behaviour of soft clay and its influence on the response of friction pile foundations. *Bull Earthq Eng* 17:1919–1939
- Grelle G, Revellino P, Guadagno FM (2011) Methodology for seismic and post-seismic stability assessment of natural clay slopes based on a viscoplastic behaviour model in simplified dynamic analysis. *Soil Dyn Earthq Eng* 31(9):1248–1260
- Haeri SM, Rajabigol M, Salaripour S, Kavand A, Sayyaf H, Afzal-soltani S, Asefzadeh A (2023) Effects of physical modeling boundary conditions on the responses of 3×3 pile groups to liquefaction induced lateral spreading. *Bull Earthq Eng* 21:2469–2502
- Hsieh SY, Lee CT (2011) Empirical estimation of the Newmark displacement from the Arias intensity and critical acceleration. *Eng Geol* 122(1–2):34–42
- Jia K, Xu C, Dou P, Zhang X, Song J (2023) Seismic behavior and failure mechanism of pile-group in mildly sloping liquefiable soils with crusts: large-scale shaking table experiment. *J Earthquake Eng* 27(15):4260–4287
- Jibson RW (2007) Regression models for estimating coseismic landslide displacement. *Eng Geol* 91(2–4):209–218
- Karray M, Hussien MN, Delisle MC, Ledoux C (2018) Framework to assess pseudo-static approach for seismic stability of clayey slopes. *Can Geotech J* 55(12):1860–1876
- Kutter BL, James RG (1989) Dynamic centrifuge model tests on clay embankments. *Géotechnique* 39(1):91–106
- Lefebvre G, Leboeuf D, Hornych P, Tanguay L (1992) Slope failures associated with the 1988 Saguenay earthquake, Quebec, Canada. *Can Geotech J* 29(1):117–130
- Lin ML, Wang KL (2006) Seismic slope behavior in a large-scale shaking table model test. *Eng Geol* 86(2):118–133
- Lin C, Wang G, Guan C, Feng DC, Zhang F (2023) Experimental study on the shear characteristics of different pile-soil interfaces and the influencing factors. *Cold Reg Sci Technol* 206:103739
- Liu Y, Zhang L (2019) Seismic response of pile-raft system embedded in spatially random clay. *Géotechnique* 69(7):638–645
- Liu C, Tang L, Ling X, Deng L, Su L, Zhang X (2017) Investigation of liquefaction-induced lateral load on pile group behind quay wall. *Soil Dyn Earthq Eng* 102:56–64
- Liu S, Zhang G, Luo F (2022) Centrifuge modeling of new pile reinforcement on slopes subjected to drawdown. *Bull Eng Geol Environ* 81(10):1–15
- Mao W, Liu B, Rasouli R, Aoyamae S, Towhata I (2019) Performance of piles with different configurations subjected to slope deformation induced by seismic liquefaction. *Eng Geol* 263:105355
- Mayoral JM, Alberto Y, Mendoza MJ, Romo MP (2009) Seismic response of an urban bridge-support system in soft clay. *Soil Dyn Earthq Eng* 29(5):925–938
- Meymand P, J (1998) Shaking table scale model tests of nonlinear soil-pile-superstructure interaction in soft clay. University of California, Berkeley
- Mi Y, Wang JH (2021) Finite-element modeling of submarine landslide triggered by seismic loading in saturated cohesive soil deposits. *Bull Eng Geol Environ* 80:951–965
- Nguyen BN, Tran NX, Han JT, Kim SR (2018) Evaluation of the dynamic p - y_p loops of pile-supported structures on sloping ground. *Bull Earthq Eng* 16:5821–5842
- Nian TK, Guo XS, Zheng DF, Xiu ZX, Jiang ZB (2019) Susceptibility assessment of regional submarine landslides triggered by seismic actions. *Appl Ocean Res* 93(12):101964
- NSPRC (National standard of the People's Republic of China) (2010) Code for seismic design of buildings. GB50011-2010. Ministry of Construction of Peoples Republic of China, Beijing
- Olgun M, Fidan B, Yenginar Y (2019) Model studies of lateral soil pressure on drilling piles in dry and saturated sands. *Soil Mech Found Eng* 56(4):280–286
- Pan R, Xu C, Jia K, Dou PF, Kamran I (2023) Large-scale shaking table test and three-dimensional numerical simulation research on earthquake seismic failure response of laterally spreading site-pile group-superstructure system. *Bull Earthq Eng* 21(10):4789–4819
- Parise M, Jibson RW (2000) A seismic landslide susceptibility rating of geologic units based on analysis of characteristics of landslides triggered by the 17 January, 1994 Northridge, California earthquake. *Eng Geol* 58(3):251–270
- Park DS, Kutter BL (2015) Static and seismic stability of sensitive clay slopes. *Soil Dyn Earthq Eng* 79:118–129
- Peng W, Zhao M, Zhao H, Yang CW (2024) Seismic stability and failure mode of the slope containing a two-pile foundation. *Bull Eng Geol Environ* 82:33
- Rodríguez-Ochoa R, Nadim F, Hicks MA (2015) Influence of weak layers on seismic stability of submarine slopes. *Mar Pet Geol* 65:247–268
- Seed HB (1968) The fourth Terzaghi lecture: landslides during earthquakes due to liquefaction. *J Soil Mech Found Div* 94(5):1053–1122
- Soriano Camelo CY, de Almeida MCF, Madabhushi SPG, Stanier SA, de Almeida MDSS, Liu HD, Borges RG (2021) Seismic centrifuge modeling of a gentle slope of layered clay, including a weak layer. *Geotech Test J* 45(1):125–144
- Soriano Camelo CY, de Almeida MCF, de Almeida MDSS, Madabhushi GSP, Stanier S (2022) Centrifuge modeling of the seismic behavior of soft clay slopes. *J Geotech GeoEnviron* 148(11):04022089
- Stamatopoulos CA, Bassanou M (2009) Mitigation of the seismic motion near the edge of cliff-type topographies using anchors and piles. *Bull Earthq Eng* 7:221–253
- Su L, Li C, Zhang C (2021) Large-scale shaking table tests on the seismic responses of soil slopes with various natural densities. *Soil Dyn Earthq Eng* 140:106409
- Tarazona SFM, de Almeida MCF, Bretschneider A, de Almeida MDSS, Escoffier S, Borges RG (2020) Evaluation of seismic site response of submarine clay canyons using centrifuge modelling. *Int J Phys Modelling Geotechnics* 20(4):224–238
- Tinawi R, Sarrazin M, Filiatrault A (1993) Influence of soft clays on the response spectra for structures in eastern Canada. *Soil Dyn Earthq Eng* 12(8):469–477
- Tsinidis G, Rovithis E, Pitilakis K, Chazelas JL (2016) Seismic response of box-type tunnels in soft soil: experimental and numerical investigation. *Tunn Undergr Space Technol* 59:199–214
- Updike RG, Olsen HW, Schmoll HR, Kharaka YK, Stokoe KH (1988) Geologic and geotechnical conditions adjacent to the Turnagain Heights landslide, Anchorage, Alaska. Department of the Interior, US Geological Survey
- Wang LP, Zhang G (2014) Centrifuge model test study on pile reinforcement behavior of cohesive soil slopes under earthquake conditions. *Landslides* 11(2):213–223
- Wang LP, Zhang G, Zhang JM (2010) Nail reinforcement mechanism of cohesive soil slopes under earthquake conditions. *Soils Found* 50(4):459–469
- Wang Y, Zheng T, Sun R, Sun ZL, Xie ZN, Shan ZD, Liu HS, Qi WH, Bai Y (2024) Influence of the anchor angle on the seismic response of anchored stabilizing piles: centrifuge modeling tests. *Soil Dyn Earthq Eng* 180:108575
- Won J, You K, Jeong S, Kim S (2005) Coupled effects in stability analysis of soil-pile systems. *Comput Geotech* 32(4):304–315
- Wu Q, Ding X, Chen Z, Zhang Y (2022) Shaking table tests on seismic responses of pile-soil-superstructure in coral sand. *J Earthquake Eng* 26(7):3461–3487
- Xie LB, Su L, Wan HP, Ling XZ (2022) Investigation of seismic response of liquefiable canyon ground considering topography effect. *Bull Earthq Eng* 20(12):6505–6526

- Xu X, Huang Y, Yashima A, Du XL (2022) Failure evolution process of pile-anchor reinforced rock slope based on centrifuge shaking table tests. *Eng Geol* 311:106920
- Yan K, He J, Cheng Q, Fan G, Wang ZJ, Zhang JJ (2020) A centrifugal experimental investigation on the seismic response of group-pile foundation in a slope with an inclined weak intercalated layer. *Soil Dyn Earthq Eng* 130:105961
- Yang Q, Zhu B, Hiraishi T (2021) Probabilistic evaluation of the seismic stability of infinite submarine slopes integrating the enhanced Newmark method and random field. *Bull Eng Geol Environ* 80:2025–2043
- Yenginar Y, Olgun M (2023) Optimizing installation parameters of DM columns in clay using Taguchi method. *Bull Eng Geol Environ* 82:145
- Zeng S, Liang R (2002) Stability analysis of drilled shafts reinforced slope. *Soils Found* 42(2):93–102
- Zhang L, Liu Y (2018) Seismic responses of rectangular subway tunnels in a clayey ground. *PLoS ONE* 13(10):e0204672
- Zhang J, Pu J, Zhang M, Qiu T (2001) Model tests by centrifuge of soil nail reinforcements. *J Test Eval* 29(4):315–328
- Zhang J, Wang H, Huang HW, Chen LH (2017a) System reliability analysis of soil slopes stabilized with piles. *Eng Geol* 229:45–52
- Zhang L, Goh SH, Yi JT (2017b) A centrifuge study of the seismic response of pile-raft systems embedded in soft clay. *Géotechnique* 67(6):479–490
- Zhang L, Goh SH, Liu H (2017c) Seismic response of pile-raft-clay system subjected to a long-duration earthquake: centrifuge test and finite element analysis. *Soil Dyn Earthq Eng* 92:488–502
- Zhang C, Jiang G, Su L, Lei D, Liu W, Wang Z (2020) Large-scale shaking table model test on seismic performance of bridge-pile-foundation slope with anti-sliding piles: a case study. *Bull Eng Geol Environ* 79(3):1429–1447
- Zhang C, Jiang G, Lei D, Asghar A, Su L, Wang Z (2021a) Large-scale shaking table test on seismic behaviour of anti-slide pile-reinforced bridge foundation and gravel landslide: a case study. *Bull Eng Geol Environ* 80(2):1303–1316
- Zhang L, Zhang PP, Xu DS, Zhou T (2021b) Seismic damage analysis of piled pier system constructed on soft clay ground. *J Bridge Engineering* 26(3):04020133
- Zhang X, Wang S, Liu H, Cui J, Liu C, Meng X (2024) Assessing the impact of inertial load on the buckling behavior of piles with large slenderness ratios in liquefiable deposits. *Soil Dyn Earthq Eng* 176:108322
- Zhao L, Huang Y, Hu H (2020) Stochastic seismic response of a slope based on large-scale shaking-table tests. *Eng Geol* 277:105782
- Zheng T, Sun QQ, Liu HS, Qi WH, Sun R (2024) Seismic performance of a nonhomogeneous slope reinforced by anchored piles using centrifuge tests. *Bull Eng Geol Environ* 83:64
- Zhou YG, Chen J, She Y, Kaynia AM, Huang B, Chen YM (2017) Earthquake response and sliding displacement of submarine sensitive clay slopes. *Eng Geol* 227:69–83
- Zhou HZ, Liu XN, Tan JL, Zhao JH, Gang Z (2023) Seismic fragility evaluation of embankments on liquefiable soils and remedial countermeasures. *Soil Dyn Earthq Eng* 164:107631

Publisher's Note Springer Nature remains neutral with regard to jurisdictional claims in published maps and institutional affiliations.